Check for updates

Monosaccharide coatings on nanoparticles affect protein corona formation but not the interaction with their binding receptor

Eva Clemente [ID] [1], Ruth Mateu[2], Avelino Ferreira[1], Tanja Ludtke[3,4], Hender Lopez[5], Sergio E. Moya[3], Luigi Lay[2], Mahmoud G. Soliman[1]* and Marco P. Monopoli[1]*

[1]Department of Chemistry, RCSI (Royal College of Surgeons in Ireland), Dublin, Ireland, [2]Department of Chemistry, University of Milan, Milan, Italy, [3]Center for Cooperative Research in Biomaterials (CIC biomaGUNE), Basque Research and Technology Alliance (BRTA), Donostia-San Sebastian, Spain, [4]Dpto Química Orgánica II/ Facultad de Ciencia y Tecnología, Universidad del País Vasco/Euskal Herriko Unibertsitatea, Leioa, Bizkaia, Spain, [5]School of Physics, Clinical and Optometric Sciences, Technological University Dublin, Dublin, Ireland

Surface coatings with polyethylene glycol (PEG) polymers have often been employed to improve nanoparticles (NPs) biocompatibility and extend circulation time by reducing protein adsorption. PEGylated NPs benefit from steric hindrance and repulsion effects, which are influenced by PEG molecular weight, density, and chain conformation. However, repetitive exposure to PEG can trigger acute and chronic immunological responses as a result of the development of Immunoglobulin G anti-PEG antibodies. NPs functionalisation with glycans has become an emerging approach to increase their biocompatibility as these biomolecules are highly hydrophilic, biocompatible interact with biological receptors expressed in the body, and can be conjugated, controlling their orientation. In this study, we developed a series of gold NPs (AuNPs) coated with PEG linkers of different lengths and conjugated with mannose (Man) or sialic acid (Sia) glycans, and we carried out a detailed characterisation prior to and after exposure to biological fluids to study their behaviour and protein corona formation. Our findings show that the glycan-coated NPs exhibit stabilisation after protein interaction, with Man coatings showing the lowest protein affinity and that the glycans are biologically active and capable of binding to glycan receptors (such as *Concanavalin A*) despite the presence of a complex protein environment. Results indicate that glycan modification of PEGylated NPs reduces nonspecific interactions while preserving active targeting properties, underscoring their potential for therapeutic applications.

KEYWORDS

gold nanoparticles, glycans, protein corona, colloidal stability, active targeting, PEGylation processes

Introduction

Over the past few decades, significant research efforts have been dedicated to developing multifunctional nanoparticles (NPs) to enhance their therapeutic efficacy. By tailoring their surface properties through incorporating diverse functional groups, targeting ligands, and protective coatings, researchers aimed to improve the stability, biocompatibility, and selective targeting to maximize the delivery at the site of action and minimize off-target effects (Patra et al., 2018; Ferrari, 2005; Fadeel, 2019). Despite promising clinical potential and ongoing research efforts, nanomedicine faces several challenges including accumulation in filtering organs, immunogenicity, and transformations upon exposure to biological media that can delay its clinical translation (Ferrari, 2005). A well-known challenge occurs when NPs come into contact with biological fluids like serum or human plasma (HP). Upon exposure, the NPs are quickly coated with biomolecules that exhibit a strong affinity for the NP surface, forming what is known as the biomolecular corona (Cedervall et al., 2007; Ke et al., 2017; Dawson and Yan, 2021). This corona consists of two distinct layers of proteins: a tightly bound inner layer called hard corona (HC) and an outer layer of loosely attached proteins referred to as the soft corona (SC) (Walczyk et al., 2010; Perez-Potti et al., 2021; Nel et al., 2009). It is now well established that the biomolecular corona is the real interface when NPs interact with biological species, as it can modulate interactions with cellular receptors, (Monopoli et al., 2012; Monopoli et al., 2011), while the pristine surface is generally hidden and rarely available for binding (Tenzer et al., 2013; Salvati et al., 2013; Clemente et al., 2022). Therefore, it is fundamental to carefully design NPs that are capable to diminish the proteins-NP interactions, increasing their blood circulation and targeting efficiency.

Surface functionalisation of nanomaterials is a common strategy applied to tune the material's properties to increase their biocompatibility and to change their biological fate (Sperling and Parak, 2010). NPs covered with polymers have shown great stealth features, inhibiting protein adsorption and increasing the NPs' blood circulation half-life (Bertrand et al., 2017; Pelaz et al., 2015; Veronese and Pasut, 2005). Several polymers have been used for this purpose. However, PEG remains the most widely used material, and PEGylation is the most successful strategy for attenuating corona formation. PEG can be grafted onto the NPs through covalent bonds or physical adsorption, although covalently PEGylated NPs tend to maintain better access to PEG chains within biodegradable matrices during blood circulation. (Hamidi et al., 2006).

The "stealth" properties of PEGylated NPs arise from the steric hindrance and repulsion effects caused by PEG chains, which prevent interactions with blood proteins and cells. These effects are closely related to the PEG molecular weight, as well as the density and conformation of the surface chains (Akiyama et al., 2009; Rahme et al., 2013; Knop et al., 2010). Based on these properties, PEG chains on the NP's surface can be found in 'mushroom' conformations at low surface densities and 'brush' conformations at high surface densities (Colangelo et al., 2017). The variations in PEG chain conformations and molecular weight influence their flexibility and hydrophilicity, thereby affecting their 'stealth effect' towards blood proteins and macrophages (Li et al., 2021).

Although the targeting of ligands on the surface of NPs can be shielded by the protein corona, studies have proved that this targeting capability is maintained and depends on how the ligands are conjugated to the NPs (e.g., covalently or non-covalently) and on the number of proteins attached on the NPs surface (Owens and Peppas, 2006). Therefore, to improve the NPs circulation and, the NPs should be designed with careful consideration for all the impact parameters, such as the physico-chemical properties of the NPs, the protein-binding pattern and the targeting ligand and its conjugation. Additionally, recent studies have shown that repetitive exposure to PEG leads to an immunological response as a result of the production of anti-PEG antibodies (Szebeni, 2005; Chanan-Khan et al., 2003; Mohamed et al., 2019). Hence, as a safe-by-design approach, the additional coating of PEG polymer with biomolecules can increase the polymer and NPs' biocompatibility, without affecting their properties.

General strategies rely on the conjugation of antibodies or proteins that have high biocompatibility and affinity towards a specific molecular target, usually located in the cell membrane (Salvati et al., 2013; Mout et al., 2012). However, it is often difficult to control their orientation to ensure the exposure of the binding epitopes and their binding efficiency towards the target is attenuated after the biomolecular corona formation. Our study focuses on the use of glycans, abundantly found in the body and highly expressed in HP proteins (Clerc et al., 2016). Their small size and easiness to be functionalised with selected linkers make it possible to orient them on the NP's surface, exposing them to the outer part and allowing for epitope recognition. Over the years, many glycoconjugates have been synthesized, with a particular focus on gold-NPs (AuNPs), due to their tuneable plasmonic properties, ready preparation in a wide range of sizes, relatively high chemical stability and biocompatibility, and well-established synthetic protocols (Compostella et al., 2017; Marradi et al., 2013; Yilmaz and Becer, 2015). In addition, the strong Au-S interaction makes them very suitable for PEG coating strategies with thiolated PEG (Felice and Selloni, 2004; Love et al., 2005). Herein, we have synthesised a group of PEGylated and glycosylated-AuNPs owning various properties, i.e., different monosaccharides (Man and Sia), PEG length (5,000 Da and 2,000 Da) and surface charge (from negative to positive). We have carried out a detailed biomolecular corona evaluation to assess the impact of NP characteristics on protein interaction. We show how the corona formation is dependent on NP properties, with the Man having the lowest protein interaction. We have then studied the availability and activity of Man grafted onto the NPs using Concanavalin A (Con A), a lectin with a known affinity towards Man residues. Our results prove that the glycans on the NPs are available and accessible for binding, even in the presence of a complex protein environment forming a corona on the NPs.

Materials and Methods

Materials

Prior to use, all glassware was washed with aqua Regia and rinsed thoroughly with Milli-Q water (MQ water). Trisodium citrate

dehydrate, Hydrogen tetrachloroaurate (III) hydrate ($HAuCl_4$), hexadecyltrimethylammonium chloride (CTAC), sodium borohydride (99%, $NaBH_4$), ascorbic acid (AA), poly(sodium 4-styrenesulfonate) (PSS, Mw = 70 kDa), Milli-Q water (resistivity of 18.2 MΩ cm at ca. 25°C), nitric acid (HNO_3), Trizma base (Tris), Glycine, Acrylamide/bis-acrylamide 40% solution, Sodium dodecyl sulphate (SDS), Ammonium persulphate (APS), N,N,N′,N′-Tetramethylethylenediamine (TEMED), Poly(ethylene glycol) 2-mercaptoethyl ether acetic acid (cPEG-SH, Mw = 2,100 Da (PEG 2k)), sodium hydroxide (NaOH), Methanol, 2-propanol, Phosphine buffered saline (PBS) tablets, Bovine serum albumin (≥98%, BSA), skim milk powder and Immobilon®-FL PVDF Transfer Membrane were purchased from Merck (Ireland). Sodium bicarbonate (>99.7% $NaHCO_3$) was purchased from Merck (Spain). ATTO pre-packed Sephadex column dialysis membrane, Sodium hypochlorite (10%–15% active chlorine) and Dialysis tubing (3.5 k MWCO, 16 mm) were purchased from Fisher Scientific Ireland Ltd. α-carboxy-ω-thiol-poly(ethylene glycol) (cPEG-SH, Mw = 5,000 Da (PEG 5k)) and α-methoxy-ω-mercapto PEG (mPEG-SH, Mw = 5,000 Da (mPEG)) were purchased from RappPolymer. Imperial Protein Stain and Fetal bovine serum (FBS) were purchased from Thermo Fisher Scientific (Ireland). Blue loading buffer pack was purchased from Cell Signalling Technology (Ireland). Unlabelled WGA was purchased from Vector Laboratories (U.K.). Dithiothreitol (DTT) was purchased from New England Biolabs (United States). Polyvinyl Chloride (PVC) calibration Standard was purchased from Analytik Ltd. Human plasma from 8 healthy donors (500 mL each) was received from the Irish Blood Transfusion Service. They were pooled together at an equal volume of 400 mL each to form the pooled plasma, aliquoted in 2 mL Eppendorf tubes and stored at −80°C. Most buffers were prepared manually using Milli-Q water.

Methods

Synthesis of 50 nm AuNPs

Spherical AuNPs with core diameters of nominally ca. 55 nm, were synthesized following a modified seed-mediated growth method reported by Hanske et al., 2017, with some modifications as described below.

Synthesis of Au seeds (<4 nm)

A freshly prepared solution of $NaBH_4$ (200 μL, 0.02 M) was injected into a mixture of $HAuCl_4$ (50 μL, 0.05 M) in 5 mL of CTAC (100 mM), under vigorous stirring. The solution colour changed immediately from transparent to brownish. The seed solution was stirred for 3 min at 2,000 rpm, then diluted 10 times in CTAC (100 mM) and immediately used for the next step.

Growing the seeds to 10 nm spheres

The previously prepared seed solution (900 μL) and AA (40 μL, 0.1 M) were added to 10 mL of CTAC (25 mM). Then, $HAuCl_4$ (50 μL, 0.05 M) was injected under vigorous stirring. After 10 s, the stirring was stopped, and the mixture was left undisturbed at room temperature (RT) for at least 10 min. The resulting gold nanospheres presented an LSPR band centred at 521 nm.

Growing the 10 nm AuNPs to 55 nm

The previously prepared 10 nm AuNPs (1.250 mL) were added to 500 mL of CTAC (25 mM), followed by the addition of AA (2 mL, 0.1 M). Finally, $HAuCl_4$ solution (2.5 mL, 0.05 M) was injected under vigorous stirring. After 30 s, the stirring was stopped, and the reaction was kept at RT for 1 h. After 1 h, NaClO (1 mL, 1.5%) was injected under strong stirring for 5 min. Thus, $HAuCl_4$ (0.2 mL, 0.05 M) was added to the mixture and mixed for 10 s. The stirring was stopped and the reaction was kept in the oven for homogenous warming at 35°C for at least 2 h, to ensure the completion of the oxidation process. Afterwards, the AuNPs were purified by centrifugation (9,000 rpm, 30 min) to stop the reaction and remove the free CTAC molecules. Hence, the supernatant was discarded and the AuNPs were re-dispersed in Milli-Q water and stored at RT for further use. The sample was characterized by Transmission electron microscopy (TEM), UV-vis and Dynamic light scattering (DLS).

Monosaccharide conjugation to PEG molecules

The synthesis of the monosaccharides, the scheme of the coupling reaction and the characterisation of the products are shown in Figure S1 and S2 in Supplementary Material, respectively. To a solution of HS-PEG5000-COOH (or HS-PEG2000-COOH, 1 eq.) in dry DCM (0.02 M), pentafluorophenol (PFP, 3 eq.) and 1ethyl-3-(3-dimethylaminopropyl)carbodiimide (EDC, 3 eq.) were added. The reaction progress was monitored by TLC (DCM: MeOH - 9: 1). After 48 h the excess of DCM was evaporated, and the crude was re-dissolved in cold Et_2O and centrifuged for 6 min at 6,000 rpm. The supernatant was removed, and the centrifugation process was repeated 5 times until the formation of a white HSPEG5000-COO-PFP (or HSPEG2000-COO-PFP) precipitate. The precipitate (1 eq.) was dissolved in dry DCM (0.02 M) and N,N-diisopropylethylamine (DIPEA) (3 eq.) was added, followed by dropwise addition of monosaccharides Sia (1) or Man (2) (3 eq.) previously dissolved in dry DMF. The reaction was monitored by TLC (DCM: MeOH - 8: 2), and after 36 h, the solvent was removed under vacuum. The crude product was dissolved in water and purified by Sephadex G-25.

PEGylation of AuNPs

PSS coating of CTAC-stabilized AuNPs

PEGylating of NPs was carried out according to the protocol reported by Xu et al. (2018) Briefly, the NPs were coated first with PSS, which was exchanged later with PEG (with or without glycans). For the PSS coating, a stock solution of 0.125 M (in terms of monomer units) PSS (one polymer unit ($C_8H_7NaO_3S$) has 206 g/mol molecular weight) was prepared in MQ water and stored for further use. A specific amount of PSS solution, calculated using the equations of S3 in Supplementary Material, was added to the AuNPs solution and the mixture was further stirred for 1–2 min and then left without shaking at RT for 24 h. As a result, PSS molecules are adsorbed to the CTAC-coated AuNPs forming a PSS-CTAC double layer (Gole and Murphy, 2005).

Surface exchange of PSS-CTAC-AuNPs with PEG

The PSS-stabilized AuNPs were mixed with NaOH (100 mM) for a few min before the purification. The purification was performed in 15 mL falcon tubes by adding 5 mL of AuNPs solution +5 mL of MQ, then centrifuged one time at 9,000 rpm for 30 min. After centrifugation, the particles were collected and their concentration was calculated by UV-vis, as described in the physico-chemical characterisation below. To exchange the PSS-CTAC complex, the amount of PEG was calculated according to Equation 1:

$$m_{PEG} = C_{NPs} * V_{NPs} * N_{PEG} * Mw \qquad (1)$$

m_{PEG} [g] is the mass of PEG, C_{NPs} [M] is the concentration of AuNPs, V_{NPs} [L] is the volume of the NP solution used for coating, N_{PEG} is the number of PEG/NP added ($300*10^3$ PEG/NP) and Mw [Da] refers to the molecular weight of PEG. The PEGylation was performed in a total volume of 100 mL or less, based on the total amount of AuNPs, overnight, using a gentle mixing (600 rpm). Then, the NPs were mixed with 5 mL of NaOH (100 mM) for 2 h and purified by centrifugation, at 9,000 rpm for 30 min. Every PEGylation was performed twice to ensure the complete coating of the NPs unless otherwise stated.

Biomolecular corona preparation

The blood HP used for the corona studies was obtained from the Irish Blood Transfusion Service (IBTS) at St Vincent's Hospital, Dublin. The HP was obtained from eight different donors, and the cell separation was carried out in the IBTS following protocols that were in place. The HP from the donors was pooled, aliquoted in 2 mL Eppendorf tubes and stored at − 80°C until use. The use of this biological fluid for corona studies is covered by the RCSI REC 1246b. The express consensus of the donors to use the sample specimen for research purpose was given.

On the day of the experiment, an aliquot of HP was defrosted by leaving it at RT. After typically 30 min, the sample tube was briefly vortexed and spun down for 3 min at 16,000 relative centrifugal force (RCF) at RT to pellet any potential protein aggregates that might be present in the solution. The pellet was discarded while the supernatant was kept and diluted with PBS to obtain an HP concentration of 10% (15 μL of HP in a total amount of 150 μL). AuNPs were vortexed and sonicated for 3 min, then incubated with the solution of HP at 37°C for 1 h under continuous agitation at 300 rpm. After incubation, the AuNP corona complex was pelleted from excess plasma by centrifugation at 6000 RCF, 15°C for 15 min. The supernatant was discarded and the pellet was re-suspended in 500 μL of PBS and washed by centrifugation. The washing procedure removes unbound and loosely bound proteins from the NPs. The AuNP corona complexes were obtained after 1 wash.

Physico-chemical characterisation

UV-Vis spectroscopy

UV-vis absorption spectra of the AuNPs were acquired across a range of wavelengths 400–1,000 nm with UV-Vis spectroscopy to study the progression of the synthesis, as well as the colloidal stability of NPs before and after their surface modifications. AuNPs were diluted in a total volume of 750 μL in a cuvette with a path length of 1 cm. UV–vis spectra were recorded by Agilent 8453 UV–visible spectrophotometer operating from 190 to 1,100 nm^{-1}. A blank of the medium in which the AuNPs were measured was performed before every measurement. Data were analysed and plotted using GraphPad. To calculate the concentration of AuNPs, the Lambert-Beer law was applied according to Equation 2:

$$C = \frac{A_{450} * d_f}{\varepsilon_{450} * l} \qquad (2)$$

A_{450} is the absorbance measured from the UV-Vis absorption spectroscopy at 450 nm, d_f is the dilution factor used in the sample preparation, ε_{450} [$M^{-1}cm^{-1}$] is the extinction coefficient dependent on the AuNPs size, as previously calculated by Haiss et al. (2007), L is the standard path length of 1 cm.

Transmission electron microscopy

TEM images were obtained using a Hitachi H7650 TEM operating at 100 kV with an AMT side mounted camera. The TEM sample was prepared by placing a drop (4 μL) of diluted AuNPs solution on top of a copper grid coated with a layer of carbon and left to dry at RT. TEM was used to characterise the quality of AuNPs and to measure their size. The images obtained by TEM were analysed using ImageJ and the average diameter of the AuNPs was obtained by analysing a minimum amount of 200 NPs.

Dynamic light scattering

The hydrodynamic diameter (h_d), and polydispersity index (PDI) were measured by dynamic light scattering DLS while zeta potential (ζ-potential) of AuNPs by electrophoretical mobility. All samples were equilibrated for 2 min at 25°C to ensure NP motion was due to Brownian motion and not due to any thermal gradients. For each measurement, the number of runs and their duration were automatically determined and repeated five times. The NPs were measured in MQ water or PBS using the Malvern Zetasizer Nano-ZS instrument equipped with a red He–Ne laser (k = 633 nm, 4.0 mW) under a scattering angle of 173°.

Nanoparticle tracking analysis

The diameter of the NPs was also measured through NTA using a Malvern NanoSight NS300 equipped with a focused laser beam at 488 nm (approximately 40 mW) and a ×20 magnification microscope coupled with a scientific CMOS camera. After DLS, samples were diluted around 30 times to maintain the concentration at around 10^8 NPs/mL, before being used in the NTA. In this way, the instrument was visualizing around 15–25 NPs/frame, achieving maximal size distribution information while avoiding hydrodynamic interaction, which impedes particles' movement. Each sample was recorded 3 times for 60 s each at 25°C. The sample was manually advanced between the recordings. The videos were analysed by the in-built NanoSight Software NTA 3.2 using default settings.

Differential centrifugal sedimentation

DCS experiments were performed with a CPS Disc Centrifuge DC24000 (CPS Instruments Inc.), using the standard sucrose gradient 8%–24% (w/v, density 1.064 g cm^{-3}). The analytical machine was capable of running at 24,000 RPM, analysing NPs from 2 nm to 80 μm, with the size resolution down to 0.2 nm. For these experiments, the disc speed was set to 18,000 RPM. Polyvinyl chloride particle (PVC) calibration standard (559 nm, density of 1.385 g cm^{-3}, Analytik Ltd.) was used for each sample before every measurement. The data were expressed as a relative number or weight distribution normalised by the main peak height. The data analysis is described in detail in S5 of Supplementary Material.

Agarose gel electrophoresis (AGE)

The NP electrophoretic mobility was assessed using a 1% (w/w) low melting point agarose gel in Tris EDTA Buffer. A 10× Tris EDTA buffer stock was prepared by dissolving 48.4 g Trizma Base and 20 mL 0.5 M EDTA in 1 L of MQ water. 2 g of agarose were dissolved in 200 mL of 1x Tris EDTA buffer, by heating in a microwave for 4 min. Samples were mixed with Orange G and 30 μL of the solution was loaded in each well. The electrophoresis was performed at 100 V in 1x Tris EDTA buffer for 60 min, unless differently stated, using a BioRad Agarose Electrophoretic System.

Fluorescence correlation Spectroscopy (FCS)

FCS measurements were performed with a Zeiss LSM 880 confocal microscope with Zen black software. The laser source was a HeNe 633 laser with a wavelength of 633 nm and a 40X C Apo/1.2 W DICIII with a water immersion objective. The confocal volume was estimated using ATTO 633 (25 nM) with a well-defined diffusion coefficient in water (3.3 × 10^{-6} cm^2 s^{-1}). The fluorescence from the BSA or HP proteins was detected by a photomultiplier tube (PMT) detector in the range 650–710 nm. As a control, the diffusion time of proteins was obtained by measuring 30 nM of the proteins in PBS. All measurements consisted of at least 20 runs of 10 s each. FCS data was evaluated with the open-source software QuickFit 3.0. Autocorrelation functions were fitted with a 3D diffusion model with two components, free lectin and lectin associated with AuNPs, and by using the fit algorithm Simulated Annealing and Levenberg-Marquardt.

BSA and HP proteins were fluorescently labelled following the manufacturer's instructions. Briefly, a solution of NaHCO$_3$ at pH 9 was prepared and mixed with 20 parts of PBS and the pH was adjusted to 8.3. The proteins were dissolved in the previously prepared solution and stirred. ATTO was added dropwise in a molar ratio BSA/HP-ATTO of 1:3. The solution was covered in aluminium foil and left stirring for 7 h. The solution was purified through a pre-packed Sephadex column, prepared as per the manufacturer's instructions. The obtained solution was further purified through a 10.000 MW cut-off dialysis membrane, for 2 days, under aluminium foil. The collected sample was finally lyophilized and stored at −20°C.

Nuclear magnetic resonance

NMR spectra were recorded on a Bruker Advance 400 (400 MHz) in D$_2$O as solvent, with a standard probe BBO 400 MHz S1 5 mm with Z-gradient. All chemical shifts are reported as δ in parts per million (ppm) and are relative to residual solvent peaks (D$_2$O = 4.79).

Proteomics and glycan analysis

Sodium dodecyl sulphate−polyacrylamide gel electrophoresis (SDS-PAGE)

SDS-PAGE analysis of the protein corona was carried out with the following method. Briefly, after the last centrifugation step of the biomolecular corona preparation (see above), the AuNP corona complexes were re-suspended in 12 μL of PBS and 6 μL of 3X Denaturation buffer/DTT (New England biolab) to reach the final buffer composition [62.5 mM Tris-HCL pH 6.8, 2% (w/v) SDS, 10% glycerol, 0.04 M DTT and 0.01% (w/v) bromophenol blue] and denatured at 100 °C for 5 min. The samples were then loaded in a 10% polyacrylamide gel made in the lab prior to the experiment, or in a precast gel (Mini-PROTEAN TGX Gels, 10%, Bio-rad). Gel electrophoresis was performed at 120 V, 400 mA for about 70 min each until the proteins neared the end of the gel. Gels were washed with deionised water 3 times, 5 min each before being stained with the Imperial protein stain solution (Coomassie R-250) for 1 h. Gels were then imaged with the Amersham imager 600 (GE Healthcare, Europe) in colorimetric mode and analysed through ImageJ.

Gel densitometry

The gel densitometry was performed with ImageJ for each lane. The density of the single protein bands was obtained by selecting each band peak from the plot previously obtained and dividing the calculated density by the total density of the lane, multiplied by 100. This would give us the percentage of the single protein for each sample.

Lectin binding assay

ConA lectin was dissolved in PBS at a concentration of 1 mg/mL, aliquoted and stored at −20°C. AuNPs or AuNPs-corona complexes were incubated with 35 nM of ConA in PBS, at 37°C for 1 h. After the incubation, the system was directly characterised through UV-vis, DLS, NTA and DCS as previously described.

Dot blot

2 μL of lectin or BSA were blotted onto a PVDF membrane (Sigma Aldrich, Ireland) pre-wetted with methanol and equilibrated in PBS, as per manufacturer instruction, to a final concentration of 1 μM or 10 μM. The membrane was blocked by incubating with 1% skim milk in PBS for 1 h. It was then washed 3 times with PBS and incubated with a 200 μL solution of AuNPs-corona complexes (0.1 mg/mL) for 1 h at RT. Then, the membrane was washed 3 times with PBS and scanned with the Amersham Imager 600 (GE Healthcare, Europe) in colorimetric mode.

Statistical analysis and plotting

All experiments were performed for a minimum of three independent times. Error bars were measured as the standard deviation of the mean. Were specified, normalization was performed by dividing each value of a measurement by the maximum value observed for each sample. Statistical analysis and data plotting were mainly performed in GraphPad Prism (version 9) and Excel (Office 2016).
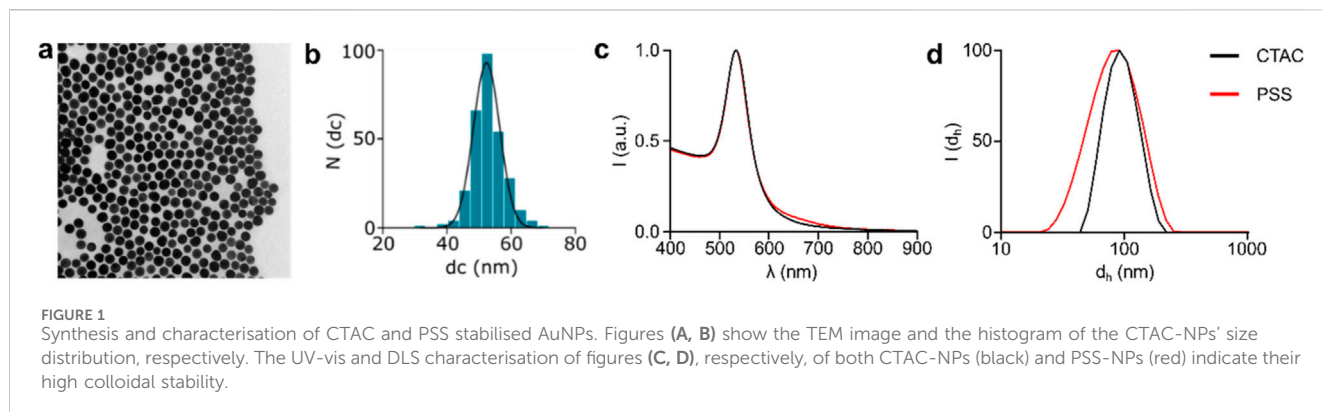
FIGURE 1
Synthesis and characterisation of CTAC and PSS stabilised AuNPs. Figures **(A, B)** show the TEM image and the histogram of the CTAC-NPs' size distribution, respectively. The UV-vis and DLS characterisation of figures **(C, D)**, respectively, of both CTAC-NPs (black) and PSS-NPs (red) indicate their high colloidal stability.

TABLE 1 DLS and DCS results of CTAC- and PSS-NPs.

	DLS			DCS
	z-av. (nm) ± SD	PDI ± SD	z-pot. (mV) ± SD	App. Size (nm) ± SD
CTAC-NPs	90.0 ± 0.2	0.09 ± 0.015	29.7 ± 0.7	45.3 ± 0.4
PSS-NPs	75.4 ± 0.3	0.15 ± 0.007	−32.6 ± 1.1	43.2 ± 0.3

Results and discussion

Synthesis and surface exchange of AuNPs

50 nm AuNPs were synthesised following a modified seed-mediated growth method developed by Hanske et al. (2017) as described in the Material and Methods and the size distribution and colloidal stability were obtained by TEM, UV-vis and DLS characterisation. AuNP size distribution appears monodisperse in shape (Figure 1A) and with an average diameter of 51.1 ± 5.1 nm (Figure 1B). UV-vis (Figure 1C) confirms the high colloidal stability in water with a Local Surface Plasmon Resonance (LSPR) peak at 533 nm, which is in agreement with the size distribution measured by TEM. The DLS analysis (Figure 1D) confirms the high monodispersity and colloidal stability, providing a hydrodynamic diameter of 90.0 ± 0.2 nm and a z-potential of 29.7 ± 0.7. (Table 1).

Given the high abundance and pivotal functions of Sia and Man in organisms, they have been selected for this study. In fact, Sia has been identified as the main component of HP glycoproteins, participating in many physiological and pathological processes, and it is the main component of the sialyl Lewis x, an O-glycan found on the surface of cells, crucial for mediating cell-cell recognition. It can specifically bind to selectins, which are highly expressed on tumour and endothelial cell surfaces. Man is an abundant monosaccharide component of N-glycans, and it has a significant influence on *in vivo* therapeutic activity. It is commonly applied in the synthesis of glycoconjugates due to its ability to target Man receptors.

α-Mercapto-ω-carboxy-PEG (cPEG) of two lengths, 5,000 Da (PEG 5k) and 2,000 Da (PEG 2k), was selected as a linker for the functionalisation with Man and Sia. The coupling of the monosaccharides to the PEGs was performed as described in Material and Methods. α-methoxy-ω-mercapto PEG of 5,000 Da (mPEG) was also used to change the overall charge of the NPs' surface.

The colloidal stability of CTAC-capped AuNPs was ensured through a two-step ligand exchange process involving initial PSS adsorption, followed by PEGylation, as previously described. (Xu et al., 2018). PSS, a negatively charged polymer, is added to the NPs solution, forming a complex with the CTAC-NPs (PSS-NPs), which can prevent particle aggregation by balancing the high positive charge of CTAC upon PEG addition. The PSS-NPs characterisation is shown in Figures 1C, D; Table 1. Then, the exposure to the thiolated PEG leads to the exchange and removal of the CTAC-PSS complex. To ensure that the NPs were fully covered by the PEG polymers, the PEGylation was performed two consecutive times. As expected, the CTAC-NPs showed a highly positive charge while the PSS- and the PEG-NPs showed a negative charge (Table 1; Supplementary Table S1). For the cm-NPs or the NPs with the double PEG, i.e., cPEG and mPEG, the cPEG or the glyco-PEG were used for the first PEGylation and mPEG for the second one. A schematic representation of the NP surface modification process with different conjugates is shown in Figure 2. The characterisation of the cm-NPs after the first PEGylation with cPEG, PEG-Sia, and PEG-Man is shown in Supplementary Table S2; Supplementary Figure S4.

Overall, nine different PEG-NP conjugates were synthesised (Figure 2), and they were characterised by UV-vis, DLS, NTA, DCS, AGE and zeta-potential (Supplementary Material). As shown in Table 2, all the NPs retained their stability during the surface exchange. As expected, a very similar size is observed for all the functionalised NPs, as calculated by DLS, NTA and DCS. The surface charge of the NPs measured via z-potential is listed in Supplementary Table S1. The pattern of the z-potential results is reflected in the AGE (Supplementary Figures S3, S4), which shows a different migration of the NPs depending on their different charge.

Protein corona formation

The glycoPEG-NPs were incubated with either BSA or HP 10% and the protein corona was characterised through UV-vis, DLS, NTA, DCS and SDS-PAGE (Supplementary Material). Table 2

FIGURE 2
Schematic representation of the NP conjugates used in this study.
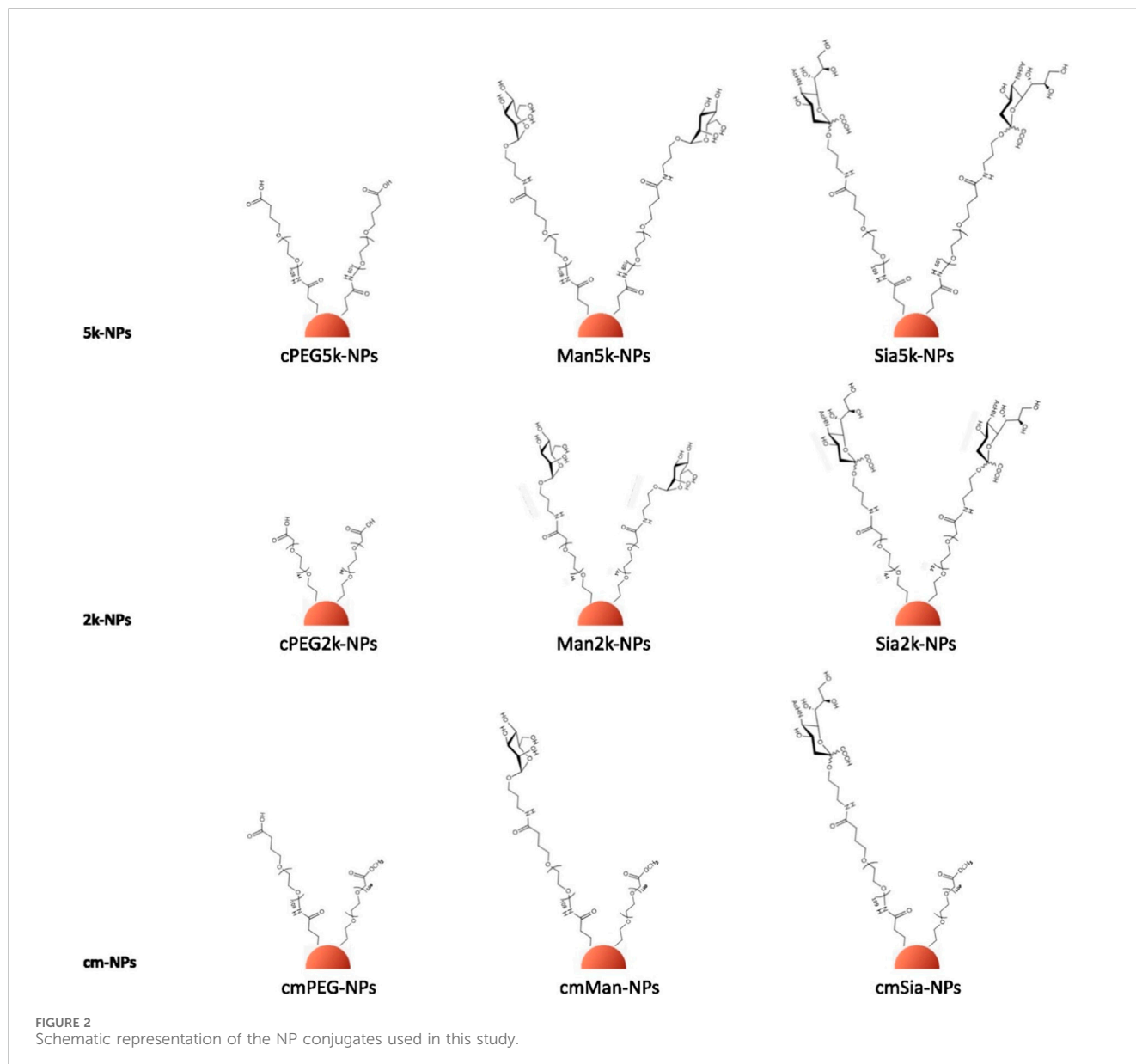
shows the full characterisation of all the NPs, in water and after corona formation with BSA and HP, through DLS, NTA and DCS. Along with evaluating changes in the physico-chemical characterisation, DCS was also used to measure the thickness of the protein corona, using the core-shell method as described in Materials and Methods. As shown in Figure 3A, the NPs' conjugation affects the protein corona formation, where Man 5k-NPs show a much lower thickness for both BSA and HP, compared to PEG 5k- and Sia 5k-NPs, indicating an interaction with less proteins. Sia 5k-NPs, instead, have the thickest HP corona, suggesting a protein attraction even higher than the plain PEG-NPs, while the thickness of these two NPs is comparable when incubated in BSA. In particular, the core-shell model calculations show a percentage of BSA almost 4 times smaller in Man 5k NPs, compared to both PEG 5k and Sia 5k-NPs, and 4 and 6 times smaller than the PEG 5k- and Sia 5k-NPs,

respectively for HP. For the 2k-NPs (Figure 3B), the BSA corona is comparable for all three NPs. With HP, however, PEG 2k-NPs show a loss of stability after the centrifugations, as shown in Supplementary Figure S7, making them difficult to be characterised.

The presence of Man and Sia leads to a stabilisation of the NPs, which show a similar corona thickness. The cm-NPs, instead (Figure 3C), show a similar corona thickness in both BSA and HP, whether the glycan is present on the NPs or not. These results suggest that the corona formation is driven by the type of glycan exposed on the NPs' surface, the length of PEG used, and the surface charge.

When the glycans were conjugated to 2k PEG length, no differences were observed with the glycan used, as a similar corona thickness was observed regardless of the applied modification. This can be due to the different conformation of

TABLE 2 NP physico-chemical characterisation with DLS, NTA and DCS in water and after corona formation with BSA and HP.

	DLS		NTA	DCS	
	z-av. (nm) ± SD	PDI ± SD	Size (nm) ± SD	App. Size (nm) ± SD	Thickness (nm) ± SD
PEG 5k					
Pristine	83.5 ± 0.6	0.12 ± 0.02	84.2 ± 1.6	41.6 ± 0.1	—
BSA	93.3 ± 0.8	0.09 ± 0.02	94.4 ± 4.0	38.9 ± 0.2	4.9 ± 0.2
HP	112.1 ± 1.4	0.13 ± 0.01	104.5 ± 6.5	38.7 ± 0.2	5.2 ± 0.2
Man 5k					
Pristine	82.9 ± 0.7	0.11 ± 0.02	82.7 ± 3.0	42.5 ± 0.2	—
BSA	92.5 ± 0.4	0.09 ± 0.01	91.7 ± 2.6	41.7 ± 0.6	1.5 ± 0.6
HP	102.7 ± 2.3	0.13 ± 0.02	90.4 ± 5.2	41.9 ± 0.2	1.3 ± 0.2
Sia 5k					
Pristine	83.7 ± 1.3	0.10 ± 0.01	84.9 ± 3.8	41.2 ± 0.6	—
BSA	92.1 ± 0.7	0.09 ± 0.02	94.1 ± 1.1	39.6 ± 0.3	4.6 ± 0.3
HP	114.7 ± 1.9	0.14 ± 0.02	104.1 ± 1.5	37.9 ± 0.4	7.4 ± 0.4
PEG 2k					
Pristine	78.0 ± 0.29	0.09 ± 0.01	80.0 ± 6.7	44.4 ± 0.5	—
BSA	87.7 ± 0.6	0.10 ± 0.01	89.0 ± 3.1	41.5 ± 0.2	4.1 ± 0.2
HP	115.7 ± 12.1	0.35 ± 0.07	122.2 ± 25.6	—	—
Man 2k					
Pristine	74.5 ± 0.64	0.12 ± 0.01	78.1 ± 3.8	44.1 ± 0.2	—
BSA	85.1 ± 0.8	0.11 ± 0.01	91.2 ± 3.2	42.6 ± 0.3	3.1 ± 0.3
HP	107.9 ± 6.5	0.24 ± 0.02	117.0 ± 10.6	39.8 ± 0.0	6.8 ± 0.1
Sia 2k					
Pristine	73.3 ± 0.73	0.11 ± 0.01	77.0 ± 3.9	44.7 ± 0.3	—
BSA	82.5 ± 0.6	0.11 ± 0.01	85.4 ± 4.4	43.3 ± 0.2	2.7 ± 0.2
HP	105.7 ± 5.8	0.23 ± 0.04	104.4 ± 18.3	39.7 ± 1.3	7.1 ±
cmPEG					
Pristine	86.2 ± 0.6	0.07 ± 0.01	86.2 ± 3.5	40.4 ± 0.4	—
BSA	92.7 ± 0.6	0.08 ± 0.01	95.6 ± 1.1	39.7 ± 0.2	2.3 ± 0.2
HP	106.7 ± 0.9	0.13 ± 0.01	105.0 ± 3.5	38.1 ± 0.5	4.9 ± 0.5
cmMan					
Pristine	86.9 ± 0.6	0.08 ± 0.02	89.6 ± 0.2	40.6 ± 0.2	—
BSA	93.0 ± 0.7	0.09 ± 0.01	96.6 ± 3.2	39.4 ± 0.1	2.3 ± 0.2
HP	104.5 ± 1.1	0.13 ± 0.02	105.9 ± 3.3	38.1 ± 0.6	4.5 ± 0.5
cmSia					
Pristine	86.5 ± 0.6	0.08 ± 0.01	88.0 ± 2.1	40.0 ± 0.3	—
BSA	93.3 ± 1.0	0.09 ± 0.02	95.5 ± 3.0	39.4 ± 0.2	2.6 ± 0.1
HP	108.5 ± 1.8	0.13 ± 0.02	107.8 ± 6.6	37.5 ± 0.5	5.8 ± 0.6

FIGURE 3
Protein corona thickness of 5k-NPs **(A)**, 2k-NPs **(B)** and cm-NPs **(C)**, calculated through a core-shell model of the apparent size obtained from the DCS measurements. Man 5k-NPs clearly show the lowest corona thickness **(A)**. When PEG 2k is used as linker **(B)** or when a cmPEG is alternated to the glyco-PEG **(C)** the amount of proteins on the NP's surface is highly increased, reaching the same thickness as Sia-NPs. The thickness of PEG 2k-NPs could not be calculated, as the NPs showed low stability.

the PEG on the NPs, hence a different packing density, meaning a different surface charge. In fact, this leads to a complete aggregation of the NPs when only PEG is grafted to the NPs, while the presence of the glycans stabilised the NPs, suggesting they play an active role in the NP-protein interaction. In addition, this difference is greatly reduced when a methoxy-PEG is added to the NPs together with the glycoPEG, suggesting that both the type of glycan and the charge affect the corona attenuation.

FCS was also applied to evaluate the protein corona formation on the glyco-NP conjugates. The technique records fluctuations in the fluorescence intensity of molecules within a confocal volume, from which the diffusion time of the molecules is obtained. In our study, we measured the diffusion of BSA and HP proteins that were fluorescently labelled with the fluorophore ATTO 633, before and after exposure of the proteins to the NPs. As the NPs alone are not labelled, they can only be detected by FCS when the labelled proteins bind to them. The advantage of FCS over other techniques is that it allows us to look at the corona in media without using centrifugation or the need for the separation of free proteins. Since in our experiment the proteins are labelled but not the NPs, we will be able to discriminate between free diffusing proteins and proteins attached to the NPs, i.e., forming a corona. Figure 4A and b show the FCS results of BSA proteins and Figures 4C, D of HP proteins. On the left are shown the normalised correlation function of the proteins in PBS before and after incubation with the NPs. The diffusion time of free BSA and HP proteins in PBS is shorter than the diffusion time of the proteins in the presence of the NPs (Table 3), indicating protein binding to the NPs. Further data analysis of the fitting of the correlation function allowed the estimation of the bound and unbound protein fractions to the NPs (right), whose results are listed in Table 3. In particular, the BSA corona shows a comparable fraction of proteins in the three NPs, of between 13% and 16%. Although the thickness as shown in Figure 4 a much lower protein corona for the Man 5k-NPs compared to the other NP's functionalisation. With the HP, instead, there is a stronger difference between the three NPs, with the Man 5k-NPs confirming the lowest percentage of proteins attached of about 12.7%, compared to the 16.5% of the PEG 5k-NPS and the 25.5% of the Sia 5k-NPs. FCS corroborates results from other techniques and shows a larger corona forming on Sia NPs.

Active targeting and accessibility of Man

Single biomolecular interactions play a crucial role in the active targeting of mannosylated NPs, as the high-affinity binding between Man on the NP surface and Man receptors on immune cells, such as dendritic cells, allows for precise delivery. (Lostao et al., 2023). This targeted interaction enhances the NPs' ability to tailor the immunogenicity response, promoting specific immune activation, improving antigen presentation, and potentially leading to more effective vaccines or immunotherapies by modulating the immune system in a controlled manner. (Read et al., 2022). To investigate the accessibility and targeting efficiency of the Man grafted on the NPs, Con A, a Man-binding plant lectin, was used to probe mannosylated NPs.

Man-NPs, together with PEG-NPs used as control, were dissolved in a solution of PBS containing the lectin, and directly characterised through UV-vis (Figure 5), DLS, DCS and dot blot (Supplementary Material). To ensure that possible aggregations were due to the presence of lectins and not for the ions in the solution, the NPs were incubated alone in PBS in the same conditions and used as controls. All NPs were stable in PBS.

Figure 5 shows the UV-vis of the PEG-NPs (left columns) and Man-NPs (right columns) before and after incubation with Con A. Upon incubation of the PEG-NPs in the Con A solution (Figure 5A), their stability was not affected, since the UV-vis spectra is almost completely superimposable to the spectra of the NPs in PBS. This suggests that the Con A did not bind to the NPs, not having any affinity towards the cPEG or mPEG. When the Man-NPs are used instead, they completely aggregate and precipitate almost immediately, easily observable with the naked eye, showing a clear flattening of the UV-vis peak. While Man 5k-NPs and Man 2k-NPs show an almost flat line, due to the complete precipitation of the NPs, cmMan-NPs still present a weak and broad peak due to the presence of aggregates of NPs in solution. This lower interaction of cmMan NPs, compared to Man 5k and Man 2k NPs, is possibly due to the lower number of Man present on the NPs, as a consequence of the second PEGylation with mPEG. These findings show a clear and strong interaction between Man-NPs and ConA, proving that Man is available and
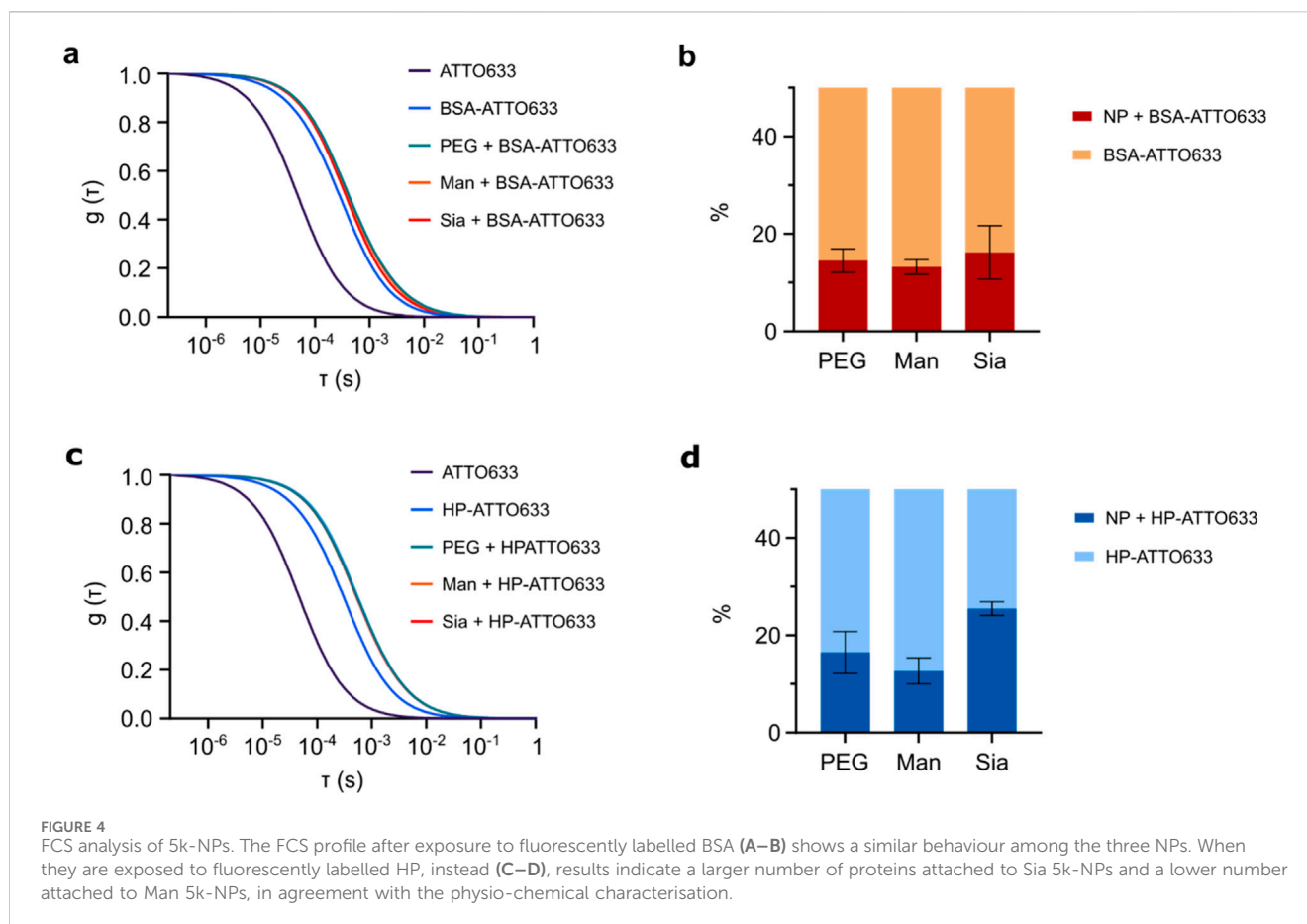
FIGURE 4
FCS analysis of 5k-NPs. The FCS profile after exposure to fluorescently labelled BSA (A–B) shows a similar behaviour among the three NPs. When they are exposed to fluorescently labelled HP, instead (C–D), results indicate a larger number of proteins attached to Sia 5k-NPs and a lower number attached to Man 5k-NPs, in agreement with the physio-chemical characterisation.

TABLE 3 Data obtained from the fitting of the correlation function for BSA and HP proteins association with the 5k-NPs. τ is the diffusion time, Dc the diffusion coefficient and dc the hydrodynamic diameter of the fluorescence species.

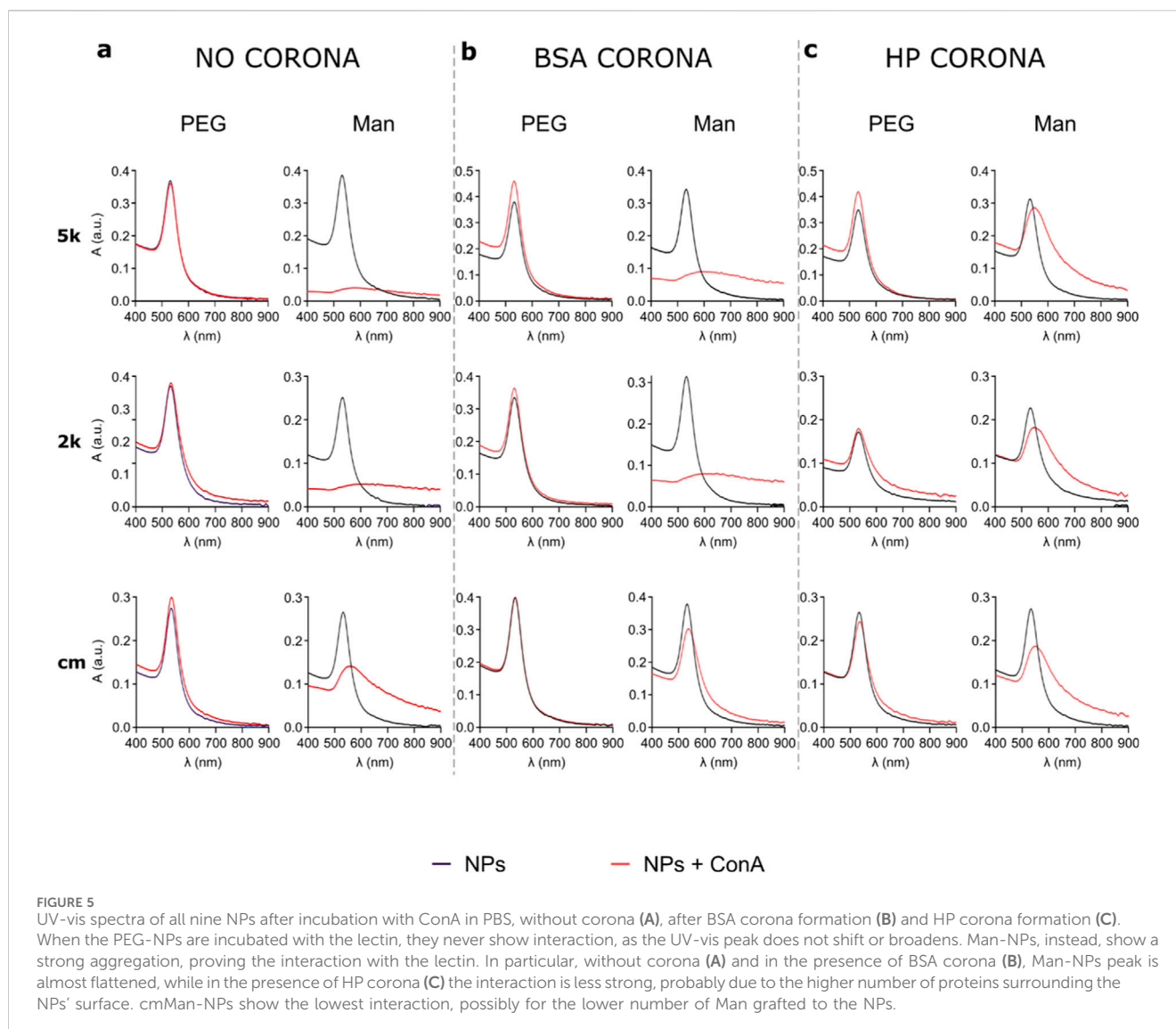|	τ [μs]	Dc [μm2·s-1]	d_C [nm]	%
Free BSA				
PEG BSA	2,108.1 ± 123.9	7.9 ± 0.4	66.4 ± 5.2	14.5 ± 2.4
Man BSA	2,136.4 ± 255.9	7.7 ± 0.4	55.7 ± 2.5	13.2 ± 1.5
Sia BSA	2083.4 ± 194.2	8.0 ± 0.8	55.1 ± 5.0	16.2 ± 5.5
Free HP				
PEG HP	2,312.9 ± 84.4	8.1 ± 0.8	54.9 ± 2.8	16.5 ± 4.3
Man HP	2,256.9 ± 583.3	8.0 ± 0.8	54.2 ± 5.5	12.7 ± 2.7
Sia HP	2,558.4 ± 272.3	7.5 ± 0.2	57.4 ± 1.9	25.5 ± 1.4

biologically accessible for binding, with a PEG length of both 5 and 2 kDa.

With these results, we also evaluated whether the binding is attenuated in the presence of the corona. Thus, the BSA corona was previously formed, and then the corona-NPs were incubated with Con A and characterised (Figure 5B). Even in these conditions, PEG-NPs completely retained their colloidal stability, while the Man 5k and Man 2k NPs visibly aggregated and generated flat UV-vis spectra as a result of binding to the lectin. cmMan NPs, instead,

do not show a visible change in stability, although the UV-vis shows a red shift and a broadening of the peak, suggesting that the interaction occurred, although with lower intensity. As previously stated, this is probably due to the lower amount of Man displayed on the NPs' surface. The presence of the BSA corona, possibly hides part of the surface, further decreasing the number of Man available. Finally, the active targeting of the NPs was evaluated after HP corona formation, as shown in Figure 5C. Once more, the interaction of the lectin with the PEG-NPs is negligible. The slight broadening of the peak and red shift, suggest that only a small interaction might have occurred with the plasma proteins. All the Man-NPs, instead, show a strong aggregation attributable to the interaction with the lectin. The lower intensity of the aggregation, compared to the Man-NPs after BSA corona formation, is probably due to the higher number of proteins surrounding the NPs' surface, as previously measured (Table 2), hence possibly hiding part of the Man.

These results indicate that the Man on the NPs is available and remains biologically accessible for binding, even in presence of a complex protein rich environment. Despite the presence of proteins surrounding the NPs, the Con A is able to penetrate the corona and selectively bind the Man. All three Man-NPs showed strong interactions with the lectin, indicating that the different linker lengths did not significantly affect the interaction, contrarily to the number of Man available on the NP's surface.

FIGURE 5
UV-vis spectra of all nine NPs after incubation with ConA in PBS, without corona **(A)**, after BSA corona formation **(B)** and HP corona formation **(C)**. When the PEG-NPs are incubated with the lectin, they never show interaction, as the UV-vis peak does not shift or broadens. Man-NPs, instead, show a strong aggregation, proving the interaction with the lectin. In particular, without corona **(A)** and in the presence of BSA corona **(B)**, Man-NPs peak is almost flattened, while in the presence of HP corona **(C)** the interaction is less strong, probably due to the higher number of proteins surrounding the NPs' surface. cmMan-NPs show the lowest interaction, possibly for the lower number of Man grafted to the NPs.

Conclusion

In this study, nine different coating strategies were applied to the core of AuNPs, aiming at their functionalization with PEGylated Man and Sia and their lectin affinity, as a measure of their targeting capacities, was assessed in conditions of protein corona formation. Exposure to BSA and HP was used to evaluate the corona formation on the NPs. Combined UV-vis, DLS, NTA and DCS studies show that the length of the PEG linker, the change in surface charge and the presence of Man or Sia affect the interaction of the protein with the NPs. Interestingly, the Man 5k-NPs result to have the thinnest corona. The addition of a neutral mPEG moiety improves the corona attenuation of negatively charged PEG- and Sia-NPs. Still, it increases the corona of neutral Man-NPs, where the number of available Man on the NPs' surface is decreased, emphasising the importance of the charge and the glycan itself. These findings underline the importance of the proper design of NPs for biomedical applications. The accessibility of the glycan of the Man-NPs was evaluated through the

carbohydrate-binding protein Con A. Man-NPs showed strong specific binding with ConA, contrary to PEG-NPs. This proved that the glycans coupled to the AuNPs are biologically accessible for binding. All three Man-NPs strongly interacted with the lectin hence the different lengths of linker did not significantly affect the interaction. cmMan NPs, however, interacted to a lesser extent, probably for the lower number of Man surrounding the NP. Moreover, the Man-ConA binding was retained even in the presence of a BSA or HP corona, implying that the glycans maintained their accessibility despite the layer of proteins surrounding the NP's surface.

The use of glycans as PEG conjugates will open new opportunities for active targeting therapies while reducing unspecific interactions. Glycans, like Sia, offer a "self" recognition element that can be utilized to mask PEG structures, helping to reduce immunogenic responses associated with PEG and enhance biocompatibility. Additionally, glycans offer a novel way to deliver therapeutic agents precisely to target cells, as many cell types and tissues

express specific receptors that recognize and bind to glycans. This dual approach of achieving stealth properties while enabling targeted delivery presents a promising platform for a range of biomedical applications. Future research activities will be focused on the proof of active targeting *in vivo*, especially in cancer models and the design of drug delivery carriers with the optimal glyco PEG-functionalisation.

Data availability statement

The raw data generated for this study are available on request to the corresponding authors.

Ethics statement

The studies involving humans were approved by Royal College of Surgeons in Ireland (RCSI) - Ethics number 001246b. The studies were conducted in accordance with the local legislation and institutional requirements.

Author contributions

EC: Data curation, Investigation, Methodology, Validation, Visualization, Writing–original draft, Writing–review and editing. RM: Investigation, Writing–review and editing. AF: Investigation, Writing–review and editing. TL: Writing–review and editing, Supervision. HL: Methodology, Writing–review and editing. SM: Supervision, Writing–review and editing. LL: Supervision, Writing–review and editing. MS: Conceptualization, Supervision, Writing–review and editing. MM: Conceptualization, Supervision, Writing–review and editing.

Funding

Conflict of interest

The authors declare that the research was conducted in the absence of any commercial or financial relationships that could be construed as a potential conflict of interest.

The author(s) declared that they were an editorial board member of Frontiers, at the time of submission. This had no impact on the peer review process and the final decision.

Generative AI statement

The author(s) declare that no Generative AI was used in the creation of this manuscript.

Publisher's note

All claims expressed in this article are solely those of the authors and do not necessarily represent those of their affiliated organizations, or those of the publisher, the editors and the reviewers. Any product that may be evaluated in this article, or claim that may be made by its manufacturer, is not guaranteed or endorsed by the publisher.

Supplementary material

The Supplementary Material for this article can be found online at: https://www.frontiersin.org/articles/10.3389/fnano.2024.1505757/full#supplementary-material

References

Akiyama, Y., Mori, T., Katayama, Y., and Niidome, T. (2009). The effects of PEG grafting level and injection dose on gold nanorod biodistribution in the tumor-bearing mice. *J. Control. Release* 139 (1), 81–84. doi:10.1016/j.jconrel.2009.06.006

Bertrand, N., Grenier, P., Mahmoudi, M., Lima, E. M., Appel, E. A., Dormont, F., et al. (2017). Mechanistic understanding of *in vivo* protein corona formation on polymeric nanoparticles and impact on pharmacokinetics. *Nat. Commun.* 8 (1), 777. doi:10.1038/s41467-017-00600-w

Cedervall, T., Lynch, I., Lindman, S., Berggård, T., Thulin, E., Nilsson, H., et al. (2007). Understanding the nanoparticle–protein corona using methods to quantify exchange rates and affinities of proteins for nanoparticles. *Proc. Natl. Acad. Sci.* 104 (7), 2050–2055. doi:10.1073/pnas.0608582104

Chanan-Khan, A., Szebeni, J., Savay, S., Liebes, L., Rafique, N. M., Alving, C. R., et al. (2003). Complement activation following first exposure to pegylated liposomal doxorubicin (Doxil®): possible role in hypersensitivity reactions. *Ann. Oncol.* 14 (9), 1430–1437. doi:10.1093/annonc/mdg374

Clemente, E., Martinez-Moro, M., Trinh, D. N., Soliman, M. G., Spencer, D. I. R., Gardner, R. A., et al. (2022). Probing the glycans accessibility in the nanoparticle biomolecular corona. *J. Colloid Interface Sci.* 613, 563–574. doi:10.1016/j.jcis.2021.11.140

Clerc, F., Reiding, K. R., Jansen, B. C., Kammeijer, G. S. M., Bondt, A., and Wuhrer, M. (2016). Human plasma protein N-glycosylation. *Glycoconj. J.* 33 (3), 309–343. doi:10.1007/s10719-015-9626-2

Colangelo, E., Comenge, J., Paramelle, D., Volk, M., Chen, Q., and Lévy, R. (2017). Characterizing self-assembled monolayers on gold nanoparticles. *Bioconjugate Chem.* 28 (1), 11–22. doi:10.1021/acs.bioconjchem.6b00587

Compostella, F., Pitirollo, O., Silvestri, A., and Polito, L. (2017). Glyco-gold nanoparticles: synthesis and applications. *Beilstein J. Org. Chem.* 13, 1008–1021. doi:10.3762/bjoc.13.100

Dawson, K. A., and Yan, Y. (2021). Current understanding of biological identity at the nanoscale and future prospects. *Nat. Nanotechnol.* 16 (3), 229–242. doi:10.1038/s41565-021-00860-0

Fadeel, B. (2019). Hide and seek: nanomaterial interactions with the immune system. *Front. Immunol.* 10 (133), 133. doi:10.3389/fimmu.2019.00133

Felice, R. D., and Selloni, A. (2004). Adsorption modes of cysteine on Au(111): thiolate, amino-thiolate, disulfide. *J. Chem. Phys.* 120 (10), 4906–4914. doi:10.1063/1.1645789

Ferrari, M. (2005). Cancer nanotechnology: opportunities and challenges. *Nat. Rev. Cancer* 5 (3), 161–171. doi:10.1038/nrc1566

Gole, A., and Murphy, C. J. (2005). Polyelectrolyte-coated gold nanorods: synthesis, characterization and immobilization. *Chem. Mater.* 17 (6), 1325–1330. doi:10.1021/cm048297d

Haiss, W., Thanh, N. T. K., Aveyard, J., and Fernig, D. G. (2007). Determination of size and concentration of gold nanoparticles from UV–Vis spectra. *Anal. Chem.* 79 (11), 4215–4221. doi:10.1021/ac0702084

Hamidi, M., Azadi, A., and Rafiei, P. (2006). Pharmacokinetic consequences of pegylation. *Drug Deliv.* 13 (6), 399–409. doi:10.1080/10717540600814402

Hanske, C., Gonza, G., Hamon, C., Forment, P., Modin, E., Chuvilin, A., et al. (2017). Large-scale plasmonic pyramidal supercrystals via templated self-assembly of monodisperse gold nanospheres. *J. Phys. Chem. C* 121, 10899–10906. doi:10.1021/acs.jpcc.6b12161

Ke, P. C., Lin, S., Parak, W. J., Davis, T. P., and Caruso, F. (2017). A decade of the protein corona. *ACS Nano* 11 (12), 11773–11776. doi:10.1021/acsnano.7b08008

Knop, K., Hoogenboom, R., Fischer, D., and Schubert, U. S. (2010). Poly(ethylene glycol) in drug delivery: pros and cons as well as potential alternatives. *Angew. Chem. Int. Ed.* 49 (36), 6288–6308. doi:10.1002/anie.200902672

Li, M., Jiang, S., Simon, J., Paßlick, D., Frey, M.-L., Wagner, M., et al. (2021). Brush conformation of polyethylene glycol determines the stealth effect of nanocarriers in the low protein adsorption regime. *Nano Lett.* 21 (4), 1591–1598. doi:10.1021/acs.nanolett.0c03756

Lostao, A., Lim, K., Pallarés, M. C., Ptak, A., and Marcuello, C. (2023). Recent advances in sensing the inter-biomolecular interactions at the nanoscale – a comprehensive review of AFM-based force spectroscopy. *Int. J. Biol. Macromol.* 238, 124089. doi:10.1016/j.ijbiomac.2023.124089

Love, J. C., Estroff, L. A., Kriebel, J. K., Nuzzo, R. G., and Whitesides, G. M. (2005). Self-assembled monolayers of thiolates on metals as a form of nanotechnology. *Chem. Rev.* 105 (4), 1103–1170. doi:10.1021/cr0300789

Marradi, M., Chiodo, F., García, I., and Penadés, S. (2013). Glyconanoparticles as multifunctional and multimodal carbohydrate systems. *Chem. Soc. Rev.* 42 (11), 4728–4745. doi:10.1039/c2cs35420a

Mohamed, M., Abu Lila, A. S., Shimizu, T., Alaaeldin, E., Hussein, A., Sarhan, H. A., et al. (2019). PEGylated liposomes: immunological responses. *Sci. Technol. Adv. Mater.* 20 (1), 710–724. doi:10.1080/14686996.2019.1627174

Monopoli, M. P., Aberg, C., Salvati, A., and Dawson, K. A. (2012). Biomolecular coronas provide the biological identity of nanosized materials. *Nat. Nanotechnol.* 7 (12), 779–786. doi:10.1038/nnano.2012.207

Monopoli, M. P., Walczyk, D., Campbell, A., Elia, G., Lynch, I., Baldelli Bombelli, F., et al. (2011). Physical–Chemical aspects of protein corona: relevance to *in vitro* and *in vivo* biological impacts of nanoparticles. *J. Am. Chem. Soc.* 133 (8), 2525–2534. doi:10.1021/ja107583h

Mout, R., Moyano, D. F., Rana, S., and Rotello, V. M. (2012). Surface functionalization of nanoparticles for nanomedicine. *Chem. Soc. Rev.* 41 (7), 2539–2544. doi:10.1039/c2cs15294k

Nel, A. E., Mädler, L., Velegol, D., Xia, T., Hoek, E. M. V., Somasundaran, P., et al. (2009). Understanding biophysicochemical interactions at the nano–bio interface. *Nat. Mater.* 8 (7), 543–557. doi:10.1038/nmat2442

Owens, D. E., and Peppas, N. A. (2006). Opsonization, biodistribution, and pharmacokinetics of polymeric nanoparticles. *Int. J. Pharm.* 307 (1), 93–102. doi:10.1016/j.ijpharm.2005.10.010

Patra, J. K., Das, G., Fraceto, L. F., Campos, E. V. R., Rodriguez-Torres, M. P., Acosta-Torres, L. S., et al. (2018). Nano based drug delivery systems: recent developments and future prospects. *J. Nanobiotechnology* 16 (1), 71. doi:10.1186/s12951-018-0392-8

Pelaz, B., del Pino, P., Maffre, P., Hartmann, R., Gallego, M., Rivera-Fernández, S., et al. (2015). Surface functionalization of nanoparticles with polyethylene glycol: effects on protein adsorption and cellular uptake. *ACS Nano* 9 (7), 6996–7008. doi:10.1021/acsnano.5b01326

Perez-Potti, A., Lopez, H., Pelaz, B., Abdelmonem, A., Soliman, M. G., Schoen, I., et al. (2021). In depth characterisation of the biomolecular coronas of polymer coated inorganic nanoparticles with differential centrifugal sedimentation. *Sci. Rep.* 11 (1), 6443–6512. doi:10.1038/s41598-021-84029-8

Rahme, K., Chen, L., Hobbs, R. G., Morris, M. A., O'Driscoll, C., and Holmes, J. D. (2013). PEGylated gold nanoparticles: polymer quantification as a function of PEG lengths and nanoparticle dimensions. *RSC Adv.* 3 (17), 6085–6094. doi:10.1039/c3ra22739a

Read, B. J., Won, L., Kraft, J. C., Sappington, I., Aung, A., Wu, S., et al. (2022). Mannose-binding lectin and complement mediate follicular localization and enhanced immunogenicity of diverse protein nanoparticle immunogens. *Cell Rep.* 38 (2), 110217. doi:10.1016/j.celrep.2021.110217

Salvati, A., Pitek, A. S., Monopoli, M. P., Prapainop, K., Bombelli, F. B., Hristov, D. R., et al. (2013). Transferrin-functionalized nanoparticles lose their targeting capabilities when a biomolecule corona adsorbs on the surface. *Nat. Nanotechnol.* 8 (2), 137–143. doi:10.1038/nnano.2012.237

Sperling, R. A., and Parak, W. J. (2010). Surface modification, functionalization and bioconjugation of colloidal inorganic nanoparticles. *Philosophical Trans. R. Soc. A Math. Phys. Eng. Sci.* 368, 1333–1383. doi:10.1098/rsta.2009.0273

Szebeni, J. (2005). Complement activation-related pseudoallergy: a new class of drug-induced acute immune toxicity. *Toxicology* 216 (2-3), 106–121. doi:10.1016/j.tox.2005.07.023

Tenzer, S., Docter, D., Kuharev, J., Musyanovych, A., Fetz, V., Hecht, R., et al. (2013). Rapid formation of plasma protein corona critically affects nanoparticle pathophysiology. *Nat. Nanotechnol.* 8 (10), 772–781. doi:10.1038/nnano.2013.181

Veronese, F. M., and Pasut, G. (2005). PEGylation, successful approach to drug delivery. *Drug Discov. Today* 10 (21), 1451–1458. doi:10.1016/s1359-6446(05)03575-0

Walczyk, D., Bombelli, F. B., Monopoli, M. P., Lynch, I., and Dawson, K. A. (2010). What the cell "sees" in bionanoscience. *J. Am. Chem. Soc.* 132 (16), 5761–5768. doi:10.1021/ja910675v

Xu, M., Soliman, M. G., Sun, X., Pelaz, B., Feliu, N., Parak, W. J., et al. (2018). How entanglement of different physicochemical properties complicates the prediction of *in vitro* and *in vivo* interactions of gold nanoparticles. *ACS Nano* 12 (10), 10104–10113. doi:10.1021/acsnano.8b04906

Yilmaz, G., and Becer, C. R. (2015). Glyconanoparticles and their interactions with lectins. *Polym. Chem.* 6 (31), 5503–5514. doi:10.1039/c5py00089k